

Development of time-varying global gridded T_s - T_m model for precise GPS-PWV retrieval

Peng Jiang^{1,2}, Shirong Ye², Yin hao Lu¹, Yanyan Liu^{3,2}, Dezhong Chen², Yanlan Wu¹

¹School of Resources and Environmental Engineering, Anhui University, Hefei, Anhui, China,

²GNSS Research Center, Wuhan University, Wuhan, Hubei, China,

³Shenzhen Key Laboratory of Spatial Smart Sensing and Services, College of Civil Engineering, Shenzhen University, Shenzhen, Guangdong, China

Correspondence to: Peng Jiang (jiangpeng@ahu.edu.cn)

Abstract: Water-vapor-weighted mean temperature, T_m , is the key variable to estimate mapping factor between GPS zenith wet delay (ZWD) and precipitable water vapor (PWV). In near real-time GPS-PWV retrieving, estimating T_m from surface air temperature T_s is a widely used method because of its high temporal resolution and a fair degree of accuracy. Based on the T_m estimates and the extracted T_s parameters at each reanalysis grid node of ERA-Interim data, we analyzed the relationship between T_m and T_s without smoothing of data. The analysis demonstrates that T_s - T_m relationship has significant spatial and temporal variations. Then static and time-varying global gridded T_s - T_m equations were established and evaluated by comparisons with radiosonde data at 758 radiosonde stations in the Integrated Global Radiosonde Archive (IGRA). Results show that our global gridded T_s - T_m equations have prominent advantages over other globally applied models. Large biases of Bevis equation or latitude-related linear model at considerable stations are removed in gridded T_s - T_m estimating models. Multiple statistical tests at 5% significance levels show that time-varying global gridded model is superior to other T_m models at 60.15% radiosonde stations, while the second-best model, GPT2w model, is superior at only 12.7% sites. No model is significantly better at 6.20% sites. GPS-PWV retrievals using different T_m estimates were compared at 74 IGS stations. At most sites, the relative differences of GPS-PWVs are within 1% with the application of time-varying global gridded T_s - T_m equations. Such results are superior to other T_m estimation models. The differences between GPS-PWVs and radiosonde PWVs are influenced by other comprehensive factors instead of a single T_m parameter. However, evident improvements still exist at particular site by using more precise T_s - T_m equations. PWV errors could decrease by more than 30% during wetter seasons.

删除的内容: analyses of the relationship between T_m and T_s were performed

删除的内容: Analyses

删除的内容: of

删除的内容: second best

批注 [jiang1]: Abstract revised

删除的内容: By application of time-varying global gridded T_s - T_m equations

删除的内容: at most sites

删除的内容: obviously

删除的内容: special

35 1. Introduction

Water vapor is an important trace gas and one of the most variable components in the troposphere. Water vapor's transport, concentration, and phase transition directly involve in atmospheric radiation and the hydrological cycle, leading to its key role in many climate changes and weather processes (Song et al., 2016; Mahoney et al., 2016; Adler et al., 2016). It is always a challenge to measure water vapor content accurately and timely due to its small amount and high spatial-temporal variability.

40 For decades, several methods have been studied, such as radio sounding, water vapor radiometer, sun photometers, GPS and others (Ciesielski et al., 2010; Perez-Ramirez et al., 2014; Li et al., 2016; Campmany et al., 2010; Liu et al., 2013). Compared with traditional water vapor observations, ground-based GPS water vapor measurement has advantages, for example, high accuracy, high spatial-temporal resolution, all-weather availability, and low-cost (Pacione and Vespe, 2008; Haase et al., 2003; Lee et al., 2010; Means, 2013; Lu et al., 2015). Therefore, ground-based GPS water vapor products, mainly including
45 precipitable water vapor (PWV) and slant water vapor (SWV), are widely used in many fields such as real-time vapor monitoring (Karabatic et al., 2011), weather and climate research (Van Baelen and Penide, 2009; Adams et al., 2017), numerical weather prediction (NWP) (Rohm et al., 2014), and so on. However, besides GPS observations, it requires some other kinds of meteorological elements to sense PWV/SWV at each GPS station remotely. Saastamoinen model is extensively adopted to compute zenith hydrostatic delay (ZHD), and surface pressure P_s is essential in the model equation (Saastamoinen, 1972).
50 Then zenith wet delay (ZWD) is generated by deducting ZHD from zenith total delay (ZTD), and ZTD can be directly estimated from precise GPS data processing. Finally, a conversion factor Π , which is used to map ZWD onto PWV, is determined by water-vapor-weighted mean temperature T_m over a GPS station. Mapping function from ZWD to PWV is expressed as (Bevis et al., 1992):

$$PWV = \Pi \cdot ZWD = \Pi \cdot (ZTD - ZHD) \quad (1)$$

55 and Π is computed using following formula:

$$\Pi = \frac{10^6}{\rho_w R_v [(k_3 / T_m) + k_2]} \quad (2)$$

删除的内容: S

删除的内容: for decades,

删除的内容: in

删除的内容: remotely

where ρ_w is the density of liquid water, R_v is the specific gas constant for water vapor, $k_2'=(17\pm 10)\text{K}\cdot\text{mbar}^{-1}$ and $k_3=(3.776\pm 0.014)\times 10^5\text{K}^2\cdot\text{mbar}^{-1}$ are physical constants (Sheng et al., 2013).

According to previous studies, error in T_m has significant influence upon the retrieval accuracy of PWV. The approximate relationship between the relative error of PWV and T_m is(Wang et al., 2005):

$$\frac{\Delta PWV}{PWV} \approx \frac{T_m + \Delta T_m}{T_m} - 1 = \frac{\Delta T_m}{T_m} \quad (3)$$

There are three main approaches to estimate T_m . They have respective advantages and disadvantages when applying to different applications:

(1) Integral of vertical temperature and humidity profiles are believed to be the most accurate method. The profile data can be extracted from radio sounding or NWP datasets(Wang et al., 2016). However, some inconveniences have to be endured.

It usually costs considerable time to acquire NWP data, which is normally released every 6 hours with large volumes. This limits the use of NWP data in near real-time GPS-PWV retrieving. However, another data source, radiosonde data, have low spatial and temporal resolution. At most of the radiosonde sites, sounding balloons are daily cast at 00:00 UTC and 12:00 UTC. Furthermore, lots of GPS stations are not located close enough to any radio sounding site. For these GPS stations, no radiosonde data can be obtained. Therefore such methods are appropriate for climate research or long-term PWV trends study but not meet real-time requirements.

(2) Several global empirical models of T_m are established based on analyses of T_m time series from NWP datasets or other sources (Chen et al., 2014; Yao et al., 2012; Bohm et al., 2015). T_m at any time and any location can be estimated from these models independent of real meteorological observations. But some important real T_m variations, which may be dramatic during some extreme weather events, can be lost without constraints of real data. So these modeled T_m estimates are not accurate enough for high-precise meteorological applications, such as providing GPS-PWV estimates for weather predictions, etc.

(3) Many studies indicated that T_m parameter has relationships with some surface meteorological elements (e.g. surface air temperature T_s). These surface meteorological parameters can be measured accurately and rapidly. T_m then is estimated in real time using these surface measurements. For example, Bevis introduced Bevis T_s - T_m equation, $T_m=0.72\times T_s+70.2$,

删除的内容: , which

删除的内容: , for

删除的内容: is

删除的内容: A

删除的内容: however

删除的内容: of

删除的内容: ed

删除的内容: numerical

删除的内容: evident

according to analyzing 8712 radiosonde profiles collected at 13 sites in the U.S. over two years(Bevis et al., 1992), and this equation has been widely used in many other studies.

95 According to Rohm's research (Rohm et al., 2014), GPS-ZTD can be estimated very precisely by real-time GPS data processing. This means that T_m is a key parameter in near real-time GPS-PWV estimation. On the other hand, method (3) is the most suitable means to estimate T_m in near real-time because of its balance between timeliness and accuracy. However, the relationship between T_m and T_s varies with location and time. Several regional T_s - T_m equations were established using profile data over corresponding fields (Wang et al., 2012). But it is not precise enough to apply the same T_s - T_m model in a vast field, e.g., in Indian region(Singh et al., 2014). Besides this, there are some other vast areas, for example over the oceans, without high-precision specific T_s - T_m equations, and there exist significant differences between the oceanic and terrestrial atmospheric properties. It is necessary to model T_s - T_m relationship over sea region, since several ocean-based GPS meteorology experiments demonstrated the potential of such technique to retrieve PWV over the broad ocean (Rocken et al., 2005;Kealy et al., 2012). A global gridded T_s - T_m model has been established by smoothing T_m data from "GGOS Atmosphere" and T_s data from ECMWF reanalysis data in Lan's study(Lan et al., 2016). The model has relatively lower spatial resolution with $4^\circ \times 5^\circ$, however, its statistic and the estimated T_m residuals due to time variations are not fixed (Yao et al., 2014a).

删除的内容: And

删除的内容: still

删除的内容: large

删除的内容: were carried out and

删除的内容: , which

删除的内容: is

Table 1. Main differences between T_s - T_m model developed in this study and other global used T_s - T_m models

| Strategies T_s - T_m Models | Bevis model (Bevis et al., 1992) | Latitude-related linear model (Yao et al., 2014b) | Global-gridded model (Lan et al., 2016) | Time-varying global gridded model (our study) |
|-----------------------------------|----------------------------------|---|---|---|
| Applicable Regions | Regional/Global | Global | Global | Global |
| Data Sources | Radiosonde | T_s from $0.75^\circ \times 0.75^\circ$ ERAI, and T_m from $2^\circ \times 2.5^\circ$ "GGOS Atmosphere" | T_s from $0.75^\circ \times 0.75^\circ$ ERAI, and T_m from $2^\circ \times 2.5^\circ$ "GGOS Atmosphere" | T_s and T_m both from $0.75^\circ \times 0.75^\circ$ ERAI |
| Data Processing | Integrate radiosonde profiles | $4^\circ \times 5^\circ$ Sliding window smooth | $4^\circ \times 5^\circ$ Sliding window smooth | Integrate ERA-Interim profiles |
| Variations in model | Static without any variations | Spatial variations depend on only latitude(15° latitude interval), but no temporal variations | $4^\circ \times 5^\circ$ global gridded, but no temporal variations | $0.75^\circ \times 0.75^\circ$ global gridded and considering time variations |

The objective of this study is mainly to (1) develop global gridded T_s - T_m models without any spatial smooth of data and assess their precisions, and (2) study the performances of GPS-PWV retrievals using our T_s - T_m models. Table (1) lists the main differences between the T_s - T_m model developed in this study and other global used T_s - T_m models. In section 2, the data sources and T_m determining methods are introduced in detail. Then in section 3, we analyze the T_s - T_m relationships and their variations on a global scale. Global-gridded T_s - T_m estimating models in different forms are established and evaluated in section 4. Section 5 compares different PWV retrievals and section 6 presents conclusions based on our experiments.

删除的内容: ;

删除的内容: T

删除的内容: are listed in Tab. (1)

2. Data Sources and Methodology of T_m Determination

2.1 T_m Definition

T_m is defined as a function related to temperature and water vapor pressure. It can be approximated as following formula(Bevis et al., 1992):

$$T_m = \frac{\int \frac{e}{T} dz}{\int \frac{e}{T^2} dz} \approx \frac{\sum_{i=1}^n \frac{e_i}{T_i} \Delta z_i}{\sum_{i=1}^n \frac{e_i}{T_i^2} \Delta z_i} \quad (4)$$

where e and T respectively represent vapor pressure in hPa and temperature in Kelvin, i denotes the i th pressure level and Δz_i is the height difference of i th levels. Vapor pressure e is calculated using equation $e=e_s \times RH$, RH is the relative humidity and saturation vapor pressure e_s can be estimated from temperature observations using Goff-Gratch formula (Sheng et al., 2013). For the i th level, e_i parameter at the middle height is calculated by vertically exponential interpolation of its two neighbor measurement points' water vapor pressure, while the temperature is estimated by linear interpolation. The integral intervals are from earth surface to atmospheric top.

删除的内容: s

批注 [jiang2]: Explanation added

2.2 Data sources and Methodology of T_m Determination

Equation (4) needs temperature, height and relative humidity values of several atmospheric levels through the entire atmosphere. These essential profile data can be obtained from radiosonde or NWP datasets.

We employed radiosonde data from Integrated Global Radiosonde Archive (IGRA, <ftp://ftp.ncdc.noaa.gov/pub/data/igra>) to calculate T_m . Version 2.0 of the IGRA-derived sounding parameters provides pressure, geopotential height, temperature, saturation vapor pressure, and relative humidity observations at observed levels. Bias maybe introduced if integrals were terminated at lower levels (Wang et al., 2005), so the integrals were performed up to the topmost valid radiosonde data. According to our quality control processes, some radiosonde profile data were rejected. Surface observation must be available, and top profile level should not be lower than 300 hPa standard level. Furthermore, the level number between surface and the top level should be greater than five to avoid too sparse vertical profile. At most radio sounding stations, sounding balloons are launched every 12 hours, and their ascending paths are assumed to be vertical.

Profile data including same elements are usually provided by NWP products at certain vertical levels. ERA-Interim from ECMWF provides data on a regular 512 longitude by 256 latitude N128 Gaussian grid after the grid transforming performed by NCAR's Data Support Section (DSS). On each grid node of ERA-Interim, temperature, relative humidity and geopotential at 37 isobaric levels from 1000 hPa to 1 hPa can be obtained. Dividing the geopotential by constant gravitational acceleration value ($g \approx 9.80665 \text{ m/s}^2$), we can determine the geopotential heights of surface and levels. Datasets are available at 00:00, 06:00, 12:00 and 18:00 UTC every day and has been covering a period from 1979.01 to present.

In theory, the computation of equation (4) should be operated through the entire atmosphere, and the geopotential height should be converted to the geometric height. However, vast majority of the water vapor concentrate at the troposphere. Moreover, the geopotential heights of top pressure levels in the two selected reanalysis datasets are around 30-40 km. Geopotential height is very close to geometric height in such height range. According to our computation, relative difference between them is only 0.1%~0.9%. In fact, the height difference Δz can be replaced by geopotential height difference Δh in equation (4), since the division operation can almost eliminate the difference between two different height types. The value change of T_m attributed to height replacement will extremely approximate to zero. For the convenience of calculations, we directly employed geopotential height variable to estimate T_m . In this paper, we denoted the T_m derived from ERA-Interim as T_{m_ERA} .

At each reanalysis grid node, the computation of equation (4) always starts from surface height to top pressure level. The pressure levels below surface height were rejected in the calculation. T_s is defined as the variable of "temperature at 2 meters

批注 [CW3]: Maybe or may be

删除的内容: is required to

删除的内容: levels

删除的内容: ,

删除的内容: geoid

删除的内容: ,

删除的内容: m

删除的内容: geoid

删除的内容: geometroc

删除的内容: with

above ground”, and surface water vapor pressure can be derived from “2 meter dewpoint temperature” variable in ERA-Interim. These T_s were also used in the regression analyses between T_m and T_s in the following study.

3. Correlation between T_s and T_m

175 Many studies have indicated the close relationship between T_s and T_m . However, T_m is also found to be not closely related to T_s in some other regions, e.g., in Indian zone(Raju et al., 2007). Using T_m and T_s generated from global gridded reanalysis data, we are able to study the relationship between T_s and T_m in detail.

We first carried on linear regression analyses on the four years long T_s and T_m data generated from point radiosonde data and global gridded ERA-Interim datasets. Analysis results are shown in Fig. (1). Although two datasets have different temporal
180 resolutions (12 hours for radiosonde data and 6 hours for ERA-Interim data) and spatial resolutions, both analyses agree very well with each other. Our analyses also indicate that correlation coefficients between T_s and T_m are generally related to point's latitude as well as other studies(Yao et al., 2014b). Significant positive correlation coefficients can be found in mid- and high- latitudes and reaches the maximum in Polar Regions. Then the correlation coefficients drop dramatically in low latitudes. We further analyzed the main reason for such changes. T_m variable in low latitudes is stable, so it shows independence of other
185 parameters. To study the variations of T_s and T_m , we illustrated denary logarithm values of their standard deviations in figure (2). It is evident that T_m varies much less in low latitudes. Besides latitude-related features, it is worth noting that there are obvious T_s - T_m correlation coefficient differences between lands and oceans. Analyses even demonstrate negative correlation coefficients over certain oceans, e.g., low-latitude Western Pacific, Bay of Bengal or Arabian Sea. It may be mainly attributed to the different thermodynamic properties of the underlying surface, including the transfer of water latent heat, the different specific heat capacities, etc. These properties influence the T_s greatly, leading to the significantly smaller variations of T_s over
190 the seas than over the lands. Unreliable regression analysis results may be derived by both the T_s and T_m with small variations. In figure (3), scatter plots of T_s and T_m from ERA-Interim at two locations N 0.35° E 180.00° and N 70.53° E 180.00° are given. Compared with the other point, the T_s - T_m relationship at the point near the equator, as the blue dots show, is quiet obscure since the whole variation ranges of T_s and T_m are both below 10 K. The linear regression result, as the magenta line shows,

删除的内容: .

删除的内容: ly

删除的内容: both

带格式的: 突出显示

批注 [jiang4]: Tests have been separated.

also makes less sense with low T_s - T_m correlation coefficient of only -0.0893. Besides complicated spatial variations, researches have revealed that T_s - T_m relationships also have temporal variations(Wang et al., 2005). So a good T_s - T_m model should take both spatial and temporal variations into consideration, which is the main work in the following sections.

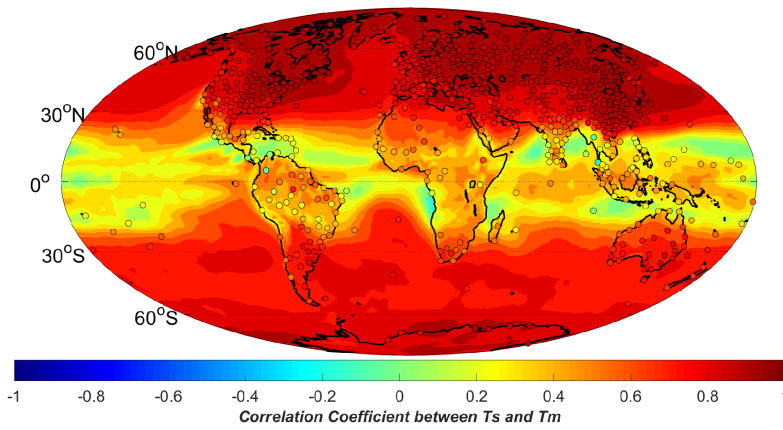
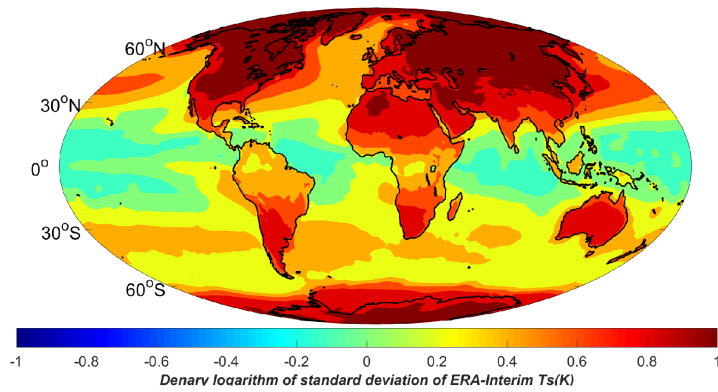


Figure 1: Correlation coefficients between T_s and T_m generated from radiosonde data (dots) and ERA-Interim reanalysis datasets (color-filled contours) over a period of 4 years from 2009 to 2012.



205

Figure 2: Denary logarithm of standard deviation of (top) T_s and (bottom) T_m generated from ERA-Interim over a period of 4 years from 2009 to 2012. Temperature unit is Kelvin.

210

Figure 3: T_s - T_m scatter plots at two locations: (blue dots) N 0.35° E 180.00° and (red dots) N 70.53° E 180.00°, the magenta and green lines are their linear fitting curves. Temperature unit is Kelvin.

批注 [jiang5]: Texts separated.

4. Developments of Global-gridded T_s - T_m models

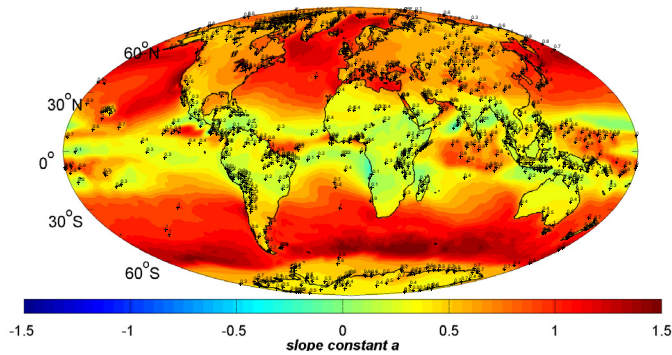
Since T_s - T_m relationship has complicated spatial variations, it is necessary to establish detailed global gridded T_s - T_m estimating equations for precise GPS-PWV remote sensing. In this section, static and time-varying global gridded T_s - T_m models are established and assessed.

215

4.1 Static global-gridded T_s - T_m model

9

Linear formulas including T_s and T_m , which is expressed as $T_m = a \times T_s + b$, are adopted in most studies, such as Bevis equation. Based on the T_s and T_m products from ERA-Interim, we performed linear fittings of T_s versus T_m on each grid point. Then slope constant (a) and intercept constant (b) of each linear expression and fitting RMSEs were calculated and contoured in figure (4). The a and b values are related to the point's latitude as well as its underlying surface. Constant a value varies from 0.6 to 0.8 when constant b about 100–50 over most continents in northern mid-high latitudes. The constants in Bevis equation, which are 0.72 and 70.2 respectively, are within such value ranges. Constant a is smaller (about 0.5–0.7) over lands in the southern mid-high latitudes. Especially, there are acute value changes of constant a and b from lands to seas in mid-high latitudes. The reason is the different variation features of T_s and T_m between seas and lands, which can be seen in figure (2). In low latitudes, a value is smaller than other regions whether over lands or oceans because of the low T_s and T_m variations. Fitting RMSEs are within 2–4 K over mid-high latitude lands, and relatively lower values over the seas or low latitude areas. The reason for the low RMSEs over the oceans around the equator is just the smaller fluctuations of T_m . Attributed to no spatial or temporal smooth of any data in our study, the precision and resolution of our static model, with no RMSE larger than 4.5 K, is clearly better than previous studies (Lan et al., 2016).



删除的内容: S

删除的内容: the a

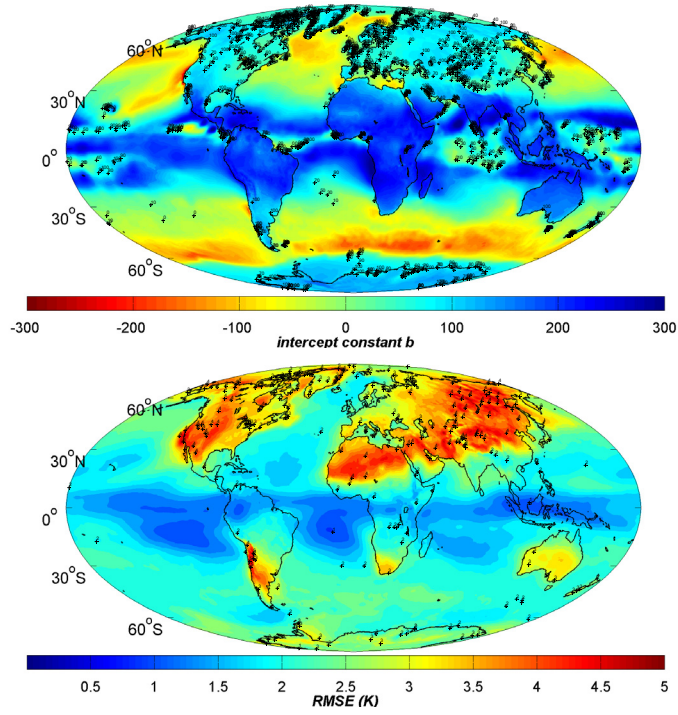


Figure 4: Distribution of (top) slope constant a , (middle) intercept constant b , and (bottom) RMSE of static linear T_s - T_m equations at ERA-Interim grid nodes. The numbers in figures are contour values. Temperature unit is Kelvin.

235

批注 [jiang6]: Explain added

4.2 Time-varying global-gridded T_s - T_m model

T_s - T_m relationship has time variations which should also be considered in precise T_s - T_m model. Therefore a time-varying equation is applied for T_s - T_m regression at each grid node:

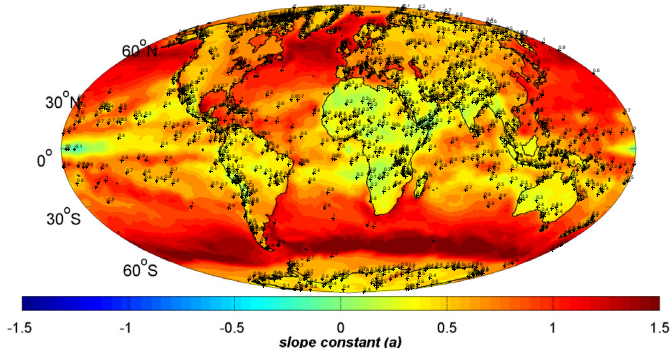
$$T_m = a \times T_s + b + m_1 \cos\left(\frac{doy}{365.25} \cdot 2\pi\right) + m_2 \sin\left(\frac{doy}{365.25} \cdot 2\pi\right) + n_1 \cos\left(\frac{doy}{365.25} \cdot 4\pi\right) + n_2 \sin\left(\frac{doy}{365.25} \cdot 4\pi\right) + p_1 \cos\left(\frac{hr}{24} \cdot 2\pi\right) + p_2 \sin\left(\frac{hr}{24} \cdot 2\pi\right) \quad (5)$$

240 where doy represents the observed day of year and hr is the observed hour in UTC time; (m_1, m_2) , (n_1, n_2) and (p_1, p_2) are the fitting coefficients of formula items to reflect amplitudes of annual, semiannual and diurnal variations in our T_s-T_m models.

Our regression indicated that the static terms in equation (5), which are determined by coefficients a and b , are similar to the static models in section 4.1 expect a little difference over some oceans. Besides a and b , we also illustrated the amplitudes of annual, semiannual, and diurnal terms. We can see that there are large annual variations (amplitude > 5 K) in the vast regions from Tibet to North Africa, and some places in Siberia and Chile, while diurnal variations (amplitude > 3 K) mainly occurs in mid-latitude lands such Northeast Asia or North America. Semiannual variations, however, are small in most areas expect some high-latitudes (amplitude > 3 K). All variations are smaller over the seas due to the slower temperature changes over waters than lands. By using time-varying T_s-T_m models the estimated T_m 's RMSEs, which are also contoured in figure (5), dropped significantly in the regions with large annual or diurnal variations.

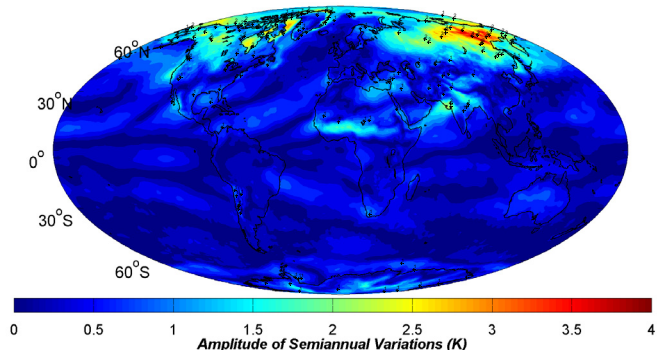
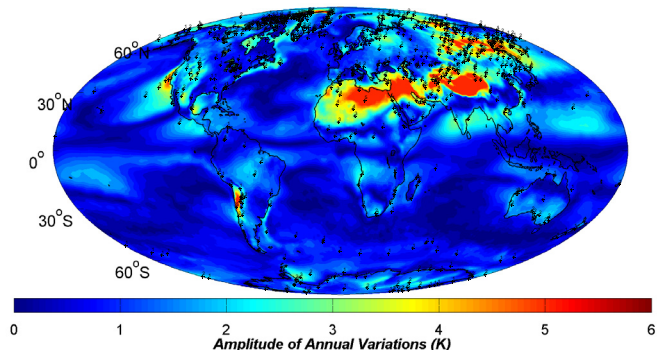
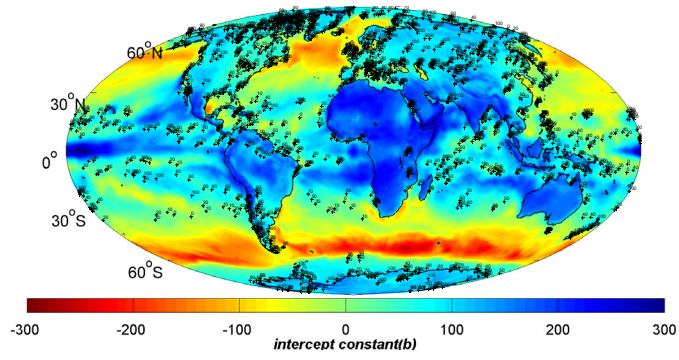
245

250



批注 [jiang7]: Explains added

删除的内容: little differences



255

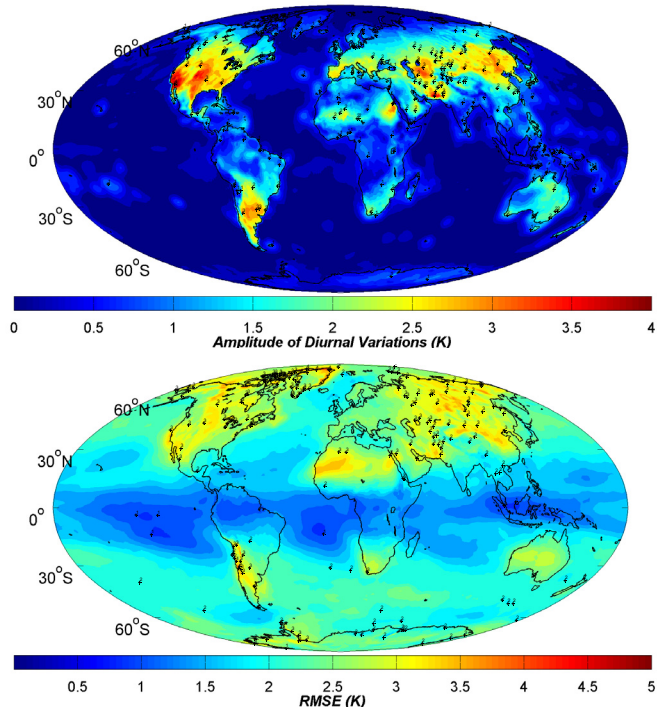


Figure 5: (top) slope constant a , (second) intercept constant b , amplitudes of T_m (third) annual, (forth) semiannual and (fifth) diurnal terms in our time-varying global gridded T_s-T_m models, and (bottom) the model estimated T_m 's RMSE distribution. The numbers in figures are contour values. Temperature unit is Kelvin.

260 **4.3 Assessments of T_s-T_m models**

In order to assess the T_s-T_m model's precisions further using other independent data sources, we generated T_m and T_s from radiosonde data at 758 radiosonde stations in the year 2016. These data are not assimilated into 2009–2012 ERA-Interim datasets. **As a result,** we can regard them as independent data to our model. At each radiosonde site, different T_s-T_m models were employed to calculate T_m . In contrast, we also estimated T_m using GPT2w model (Bohm et al., 2015), which is a global gridded T_m empirical model independent of surface meteorological observation data. Then these calculated T_m will be evaluated

265

删除的内容: , so

批注 [jiang8]: GPT2w included

by comparisons with the radiosonde's integrated T_m values (denoted as T_{m_RS}) twice a day.

The model estimated T_m are denoted as T_{m_Bevis} , T_{m_LatR} , T_{m_static} , $T_{m_varying}$ and T_{m_GPT2w} respectively from Bevis equation, Yao's latitude-related model, our static global gridded model, time-varying global gridded model and GPT2w model. When global gridded models are employed, there is a problem that a radiosonde station may not be located at a grid node. Therefore, the coefficients in T_s - T_m equations at radiosonde site's location should be horizontally interpolated from neighboring grids. The interpolation formula is expressed as (Jade and Vijayan, 2008):

$$C_{site} = \sum_{i=1}^4 w^i C_{grid}^i \quad (6)$$

C_{site} and C_{grid}^i respectively represent the coefficients in T_s - T_m equations at radiosonde site location and its neighboring grids. w^i is the interpolation coefficients, which is determined using equation:

$$w^i = \frac{(R\psi^i)^{-\lambda}}{\sum_{j=1}^4 (R\psi^j)^{-\lambda}} \quad (7)$$

where $R=6378.17$ km is the mean radius of the earth, λ is the scale factor which equals one in our study, and ψ^i is the angular distance between the i th grid node and the station's position. ψ^i is computed using following formula related to latitude φ and longitude θ :

$$\cos\psi_i = \sin\varphi_i \cdot \sin\varphi + \cos\varphi_i \cdot \cos\varphi \cdot \cos(\theta_i - \theta) \quad (8)$$

Considering the reanalysis grids are definite, and every radiosonde site is in situ, we can compute these interpolation coefficients in Eq. (6) for all radiosonde stations. Then these coefficients are stored as constants to avoid reduplicate calculation.

Taking T_{m_RS} as reference values, we calculated the bias and root mean square error (RMSE) of T_{m_Bevis} , T_{m_LatR} , T_{m_static} , $T_{m_varying}$ and T_{m_GPT2w} at each radiosonde site and illustrated them in figure (6). Obviously, Bevis equation has bad precisions in many regions with absolute bias and RMSE larger than 5 K. T_{m_LatR} can reduce estimated biases in many regions, but the

删除的内容: the

删除的内容: are not

删除的内容: any

删除的内容: d

删除的内容: , t

批注 [jiang9]: GPT2w included

RMSEs remain large. And there still exist large biases at quite a few radiosonde stations, e.g. in Africa or West Asia. T_{m_static} and T_{m_GPT2w} can remove large T_m biases at most of the radiosonde stations. $T_{m_varying}$ performs significantly better all over the world, especially in the Middle East area, North America and Siberia region, etc.

Detailed statistics of the bias's and RMSE's distributions of different models are shown in figure (7) and table (2). At over 96% radiosonde stations, biases of $T_{m_varying}$ are within -3~3 K and large positive biases (>3K) nearly disappear, while there are significant large ones in T_{m_Bevis} and T_{m_LatR} . Improvements in RMSEs are more evident, $T_{m_varying}$'s RMSEs are smaller than 4 K at over 90% radiosonde sites while few sites (<1%) have RMSEs larger than 5 K, which is clearly better than other models. In T_{m_Bevis} and T_{m_LatR} , there are more than 17% radiosonde sites have RMSE larger than 5 K. The overall performance of T_{m_GPT2w} is very close to T_{m_Bevis} except that its absolute bias is smaller than other T_m - T_m models.

删除的内容: the

删除的内容: clearly

删除的内容: significantly

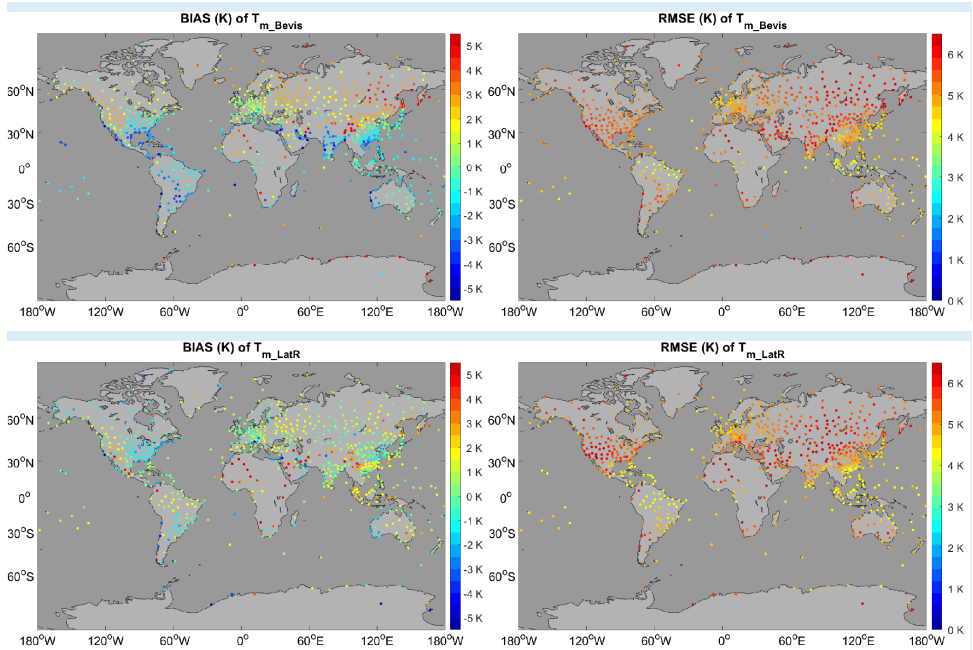
删除的内容: or

删除的内容: on

删除的内容: considerable

删除的内容: ly

批注 [jiang10]: GPT2w included



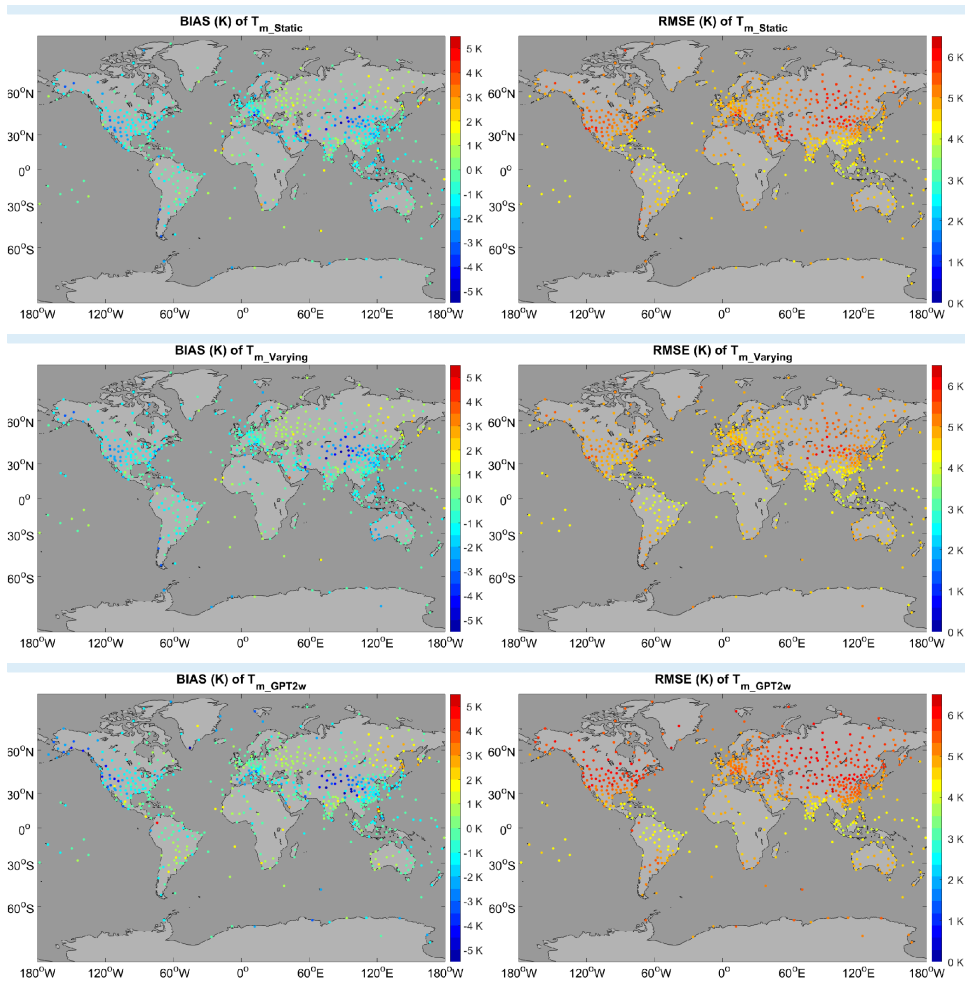


Figure 6: (left) bias and (right) RMSE of estimated T_m using T_s - T_m equations from (top) Bevis equation, (second) Yao's latitude-related model, (third) static global gridded model, (forth) time-varying global gridded model and (bottom) GPT2w model at each radiosonde station comparing with radiosonde data of the year 2016. Temperature unit is Kelvin.

批注 [jiang11]: GPT2w included

批注 [jiang12]: Figures modified

315

1) Bias distribution

2) RMSE distribution

Figure 7: (left) bias's and (right) RMSE's distributions of T_{m_Bevis} , T_{m_LatR} , T_{m_Static} , $T_{m_Varying}$ and T_{m_GPT2w} compared with respect to radiosonde data at 758 stations in 2016. Temperature unit is Kelvin.

Table 2: Statistics of T_m estimates from different T_s - T_m models and GPT2w model comparing with radiosonde T_m derivations

| Statistics | T_{m_Bevis} | T_{m_LatR} | T_{m_Static} | $T_{m_Varying}$ | T_{m_GPT2w} |
|--|----------------|---------------|-----------------|------------------|----------------|
| Average value of absolute T_m bias (K) | 1.90 | 1.31 | 1.17 | 1.13 | -0.74 |
| Average value of T_m RMSE (K) | 3.95 | 3.83 | 3.37 | 3.02 | 3.83 |
| Average relative RMSE of T_m (%) | 1.44 | 1.39 | 1.23 | 1.10 | 1.40 |
| Max Relative RMSE of mean T_m (%) | 3.69 | 4.26 | 2.57 | 2.40 | 4.31 |
| % of sites with T_m RMSE < 4 K | 55.67 | 61.35 | 75.86 | 90.11 | 53.43 |
| % of sites with T_m Relative RMSE less than 1.5% | 59.50 | 64.78 | 77.70 | 88.92 | 56.60 |

320

To verify the superior T_m estimation model at each radiosonde site, we employed the following statistical tests under the assumption of normal distribution of estimated T_m 's error:

(1) Firstly, Brown-Forsythe's tests (Brown and Forsythe, 1974) of equality of variances were carried out at each site for estimated T_m errors from two different models, e.g., model **A** and **B**. The purpose of this step is to determine that whether there is significant variance difference between two T_m results. If the test rejects the null hypothesis at 5% significance level that the errors of model **A** and **B** have the same variance, the model with smaller sample variance is regarded as the better one. However,

325

18

批注 [jiang13]: GPT2w included

批注 [jiang14]: GPT2w included

if the test doesn't reject the homogeneity of variances, analysis of variance (ANOVA) is performed in the next step.

(2) ANOVA is a technique to analyze the differences among group means (Hogg, 1987). It evaluates the null hypothesis that the samples all have the same mean against the alternative that the means are not the same. If the null hypothesis is rejected at 5% significance level, the T_m sample with smaller absolute mean value is believed to be better. Otherwise, we think that two models perform almost the same at this radiosonde site.

(3) After multiple tests and comparisons, the best model at each radiosonde stations may be determined. However, at some sites no superior model can be confirmed. So all models are believed to have equivalent performances.

Finally, we counted the number of sites at which each T_m model respectively performed superiorly, and the results are given in table (3). The time-varying global gridded model is superior to others at 456 radiosonde stations (60.16% of all sites), while the second-best estimations, T_{m_GPT2w} , is superior at only 12.66% sites.

Table 3: Number of radiosonde sites at which the five global applied T_m estimation models respectively perform superiorly

| Superior model | None | T_{m_Bevis} | T_{m_LatR} | T_{m_static} | $T_{m_varying}$ | T_{m_GPT2w} |
|-----------------|------|----------------|---------------|-----------------|------------------|----------------|
| Number of sites | 47 | 48 | 70 | 41 | 456 | 96 |

In figure (8), T_m series at IGRA station NO.62378 (N 29.8628° E 31.3492°) are given. We can see that large negative biases (< -5 K) between T_{m_Bevis} (or T_{m_LatR}) and T_{m_RS} exist, while T_{m_static} performs only slightly better from July to October. But $T_{m_varying}$ and T_{m_GPT2w} can eliminate most of the seasonal errors. Different properties of T_m series appear at another IGRA station NO.40841 (N 30.2500° E 56.9667°). Some observation data are missing, but we can still see that there are large positive differences (> 5 K) between T_{m_Bevis} (or T_{m_LatR}) and T_{m_RS} through the year. T_{m_static} 's biases are much smaller but still have some big errors in many months. The $T_{m_varying}$, however, performs as well as at NO.62378 IGRA station, with small biases and good capturing of T_m 's variations. Both time series of T_{m_GPT2w} are smooth so they cannot capture the large fluctuations of T_m time series leading to T_{m_GPT2w} 's worse accuracy than $T_{m_varying}$.

On the other hand, even $T_{m_varying}$ also have large differences from T_{m_RS} at a few IGRA stations, especially in Central Asia. It is because that our fitting analyses were based on the T_m values derived from reanalysis datasets, and reanalysis T_m did not agree well with radiosonde data at these IGRA sites during specific seasons. Improvements on reanalysis data in these regions should be performed in future.

删除的内容: s

删除的内容: At 456 radiosonde stations (60.16% of all sites)

删除的内容: , t

批注 [jiang15]: GPT2w included

删除的内容: second

批注 [jiang16]: GPT2w included and results modified

批注 [jiang17]: Text separated

删除的内容: all

删除的内容: So i

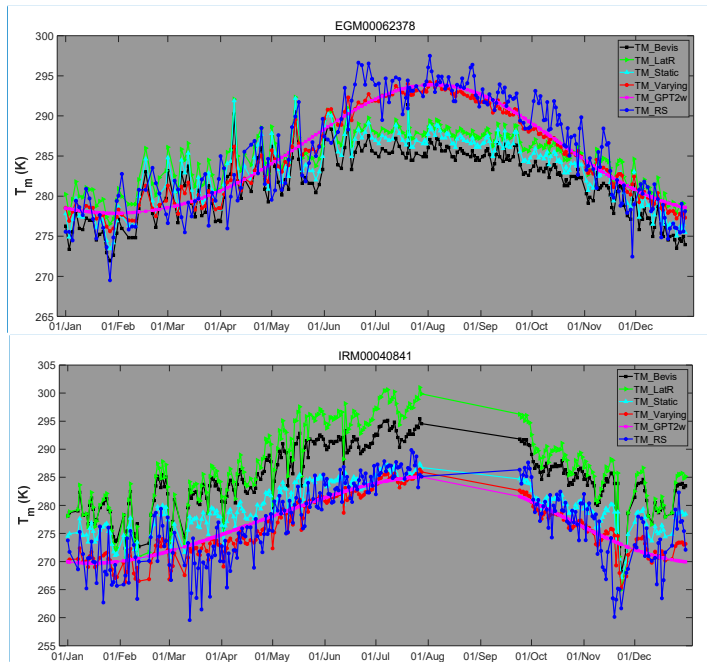


Figure 8: T_m series of T_{m_Bevis} , T_{m_LatR} , T_{m_static} , $T_{m_varying}$, T_{m_GPT2w} and T_{m_RS} at (top) EGM00062378 and (bottom) IRM00040841 IGRA sites. Temperature unit is Kelvin.

批注 [jiang18]: GPT2w included

批注 [jiang19]: GPT2w included

5. GPS-PWV retrieving experiments

GPS-PWV has different error sources with different properties, including GPS ZWD error, surface temperature and pressure measurement errors, T_m estimation error (Ning et al., 2016), and etc. It is complicated to evaluate GPS-PWV uncertainty due to the lack of collaborated additional independent techniques to monitor water vapor at GPS site. Therefore several experiments were carried out to investigate GPS-PWV precisions carefully.

删除的内容: and

5.1 Impact of T_m estimation

In order to study the actual impacts of T_m on GPS-PWV retrievals, we firstly downloaded GPS ZTD products (Byun and

删除的内容: to

370 Bar-Sever, 2009) at several IGS sites in the year 2016 from CDDIS FTP address
(<ftp://cddis.gsfc.nasa.gov/pub/gps/products/troposphere/zpd>). These selected GPS sites were equipped with meteorological
sensors so surface pressure and temperature measurements could also be obtained. ZHDs were calculated using surface
pressures and Saastamonien model. It is deduced from ZTDs to obtain ZWDs. Then T_m was generated through six approaches:
the first five T_m series were T_{m_Bevis} , T_{m_LatR} , T_{m_static} , $T_{m_varying}$ and T_{m_GPT2w} . The sixth T_m were integrated from ERA-Interim
375 profiles and interpolated to GPS site locations(Wang et al., 2016; Jiang et al., 2016). Finally, GPS-PWVs were generated from
ZWD and six different T_m estimates. We denoted these GPS-PWV sets as PWV_{BTm} , PWV_{LTm} , PWV_{STm} , PWV_{VTm} , PWV_{GTm}
and PWV_{ETm} . The only differences between these GPS-PWVs are the T_m estimates, so the impacts of other errors could be
excluded.

The T_m from ERA-Interim is believed to be the most accurate, so we regarded the PWV_{ETm} as reference values to assess
380 other PWVs. Finally, PWVs at 74 IGS sites, which have over one hundred compared points, were obtained. The relative
RMSEs of PWV_{BTm} , PWV_{LTm} , PWV_{STm} , PWV_{VTm} and PWV_{GTm} at these selected stations were calculated and illustrated in
figure (9), and detailed statistics are given in table (4). Mean relative error of all sites drops from 1.18% of PWV_{BTm} to 0.91%
of PWV_{VTm} . Obviously at most sites, PWV_{VTm} , which have minim relative errors, is prior to other PWV retrievals. At 55 sites
385 PWV_{STm} and PWV_{VTm} obtain relative RMSE smaller than 1.0%, while at only 28 sites of PWV_{BTm} , 31 sites of PWV_{LTm} and 22
sites of PWV_{GTm} perform similarly. Some relative RMSEs were remarkably reduced. For example, at ALIC site which located
in Australia with mean PWV of about 23 mm, the relative RMSE dropped from 1.97% of PWV_{BTm} to 1.10% of PWV_{VTm} . The
time series of relative differences of PWV_{BTm} , PWV_{LTm} , PWV_{STm} , PWV_{VTm} and PWV_{GTm} at ALIC station are given in figure
(10). Obviously, PWV_{BTm} and PWV_{LTm} have bigger relative errors through the year while PWV differences are significantly
390 larger only in summer season. It is attributed to the wetter atmosphere in summer than in winter. PWV_{STm} eliminates those
large differences but still retain some residual errors, which are removed more than 1.0 mm in PWV_{VTm} further. PWV_{GTm} has
some large errors during the period from May to July. All these results demonstrate that our time-varying global gridded has
precision advantages.

删除的内容: be

删除的内容: and

删除的内容: were

删除的内容: , while t

批注 [jiang20]: Reference added

删除的内容: Because t

删除的内容: are

批注 [jiang21]: GPT2w included

删除的内容: evidently

批注 [jiang22]: GPT2w included

400

Figure 9 consists of two vertically stacked bar charts. The y-axis for both is 'Relative RMSE (%)' ranging from 0 to 3.5. The x-axis is 'IGS SITES'. The top chart shows a wide distribution of RMSE values, with many sites having values between 1.0% and 2.0%, and some reaching up to 3.5%. The bottom chart shows a much more uniform and lower distribution, with most sites having RMSE values between 0.5% and 1.5%. A legend in the top right of each chart identifies five series: $PWV_{GTm} - PWV_{ETm}$ (red), $PWV_{LTm} - PWV_{ETm}$ (blue), $PWV_{STm} - PWV_{ETm}$ (magenta), $PWV_{VTm} - PWV_{ETm}$ (green), and $PWV_{GTm} - PWV_{ETm}$ (black).

Figure 9: Relative RMSEs of PWV_{BTm} , PWV_{STm} , PWV_{VTm} and PWV_{GTm} compared with PWV_{ETm} at 74 IGS stations in the year 2016

批注 [jiang23]: GPT2w included

Figure 10 consists of two vertically stacked time-series plots for the ALIC station in 2016. The x-axis for both is 'Date of 2016' from 01/Jan to 01/Dec. The top plot shows 'PWV differences (mm)' on the y-axis, ranging from -0.5 to 2.0. The data points for five different models are clustered around 0 mm, with some outliers reaching up to 2.0 mm. The bottom plot shows 'Relative errors (%)' on the y-axis, ranging from -3 to 6. The data points are clustered around 0%, with some outliers reaching up to 6%. A legend in the top right of each plot identifies the same five series as in Figure 9.

Figure 10: (top) PWV differences and (bottom) relative differences of PWV_{BTm} , PWV_{LTm} , PWV_{STm} , PWV_{VTm} and PWV_{GTm} compared with PWV_{ETm} at ALIC station in the year 2016. PWV unit is mm.

批注 [jiang24]: GPT2w included

405

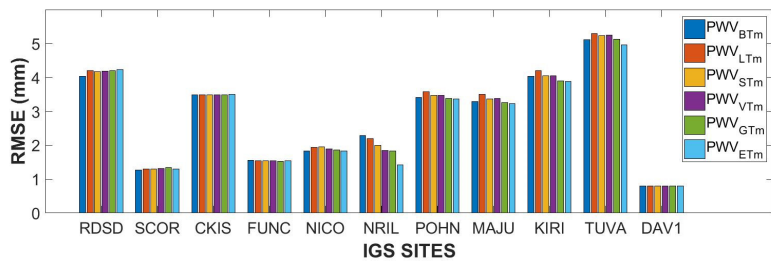
22

Table 4: Statistics about relative errors of different PWV retrievals

| Statistics | PWV _{BTm} | PWV _{LTm} | PWV _{STm} | PWV _{VTm} | PWV _{GPT2w} |
|---|--------------------|--------------------|--------------------|--------------------|----------------------|
| Mean relative RMSE of all sites | 1.18% | 1.12% | 0.93% | 0.91% | 1.32% |
| Number of sites with relative errors < 1.0% | 28 | 31 | 55 | 55 | 22 |

5.2 Comparisons between GPS-PWVs and radiosonde PWVs

Among our selected 74 IGS sites, there are only 11 sites located within 5 km to nearby IGRA radiosonde stations. At these common stations, we generated PWVs from radiosonde data (PWV_{RS}) by adjusting sounding profiles to the heights of IGS sites. It worth noticing that geoid undulation corrections should be carried out on each IGS site's geoid height (Jiang et al., 2016). Then we compared PWV_{BTm} , PWV_{LTm} , PWV_{STm} , PWV_{VTm} , PWV_{GTm} and PWV_{ETm} with PWV_{RS} . Figure (11) shows the statistics. The RMSEs of GPS-PWVs are around 1~5 mm. Comparisons indicate that at most selected sites the RMSEs of different GPS-PWV retrievals are very close (differences < 0.2 mm) regardless of the T_m sources applied. This means that other errors (e.g. ZTD estimation errors or sounding sensors errors) instead of T_m occupied the differences between GPS-PWVs and radiosonde PWVs. However, we still found obvious gaps between PWVs at NRIL (N 88.3598° E 69.3618°, 4.1km to nearby radiosonde NO.23078 sites). RMSEs decrease from 2.29 mm of PWV_{BTm} to 1.84mm of PWV_{VTm} and 1.42 mm of PWV_{ETm} . As shown in figure (12), the large PWV differences mainly appeared from May to September. During such five months, mean GPS-PWV differences to PWV_{RS} decreased by over 30% from 2.52 mm of PWV_{BTm} to 1.67 mm of PWV_{VTm} . The accuracy of PWV_{GTm} is close to PWV_{VTm} at this site, and it indicates that the spatiotemporal variations of T_m are also modeled very well by GPT2w model.



批注 [jiang25]: GPT2w included and results modified

删除的内容: Statistics are shown in f

删除的内容:

删除的内容: , which

批注 [jiang26]: Texts separated

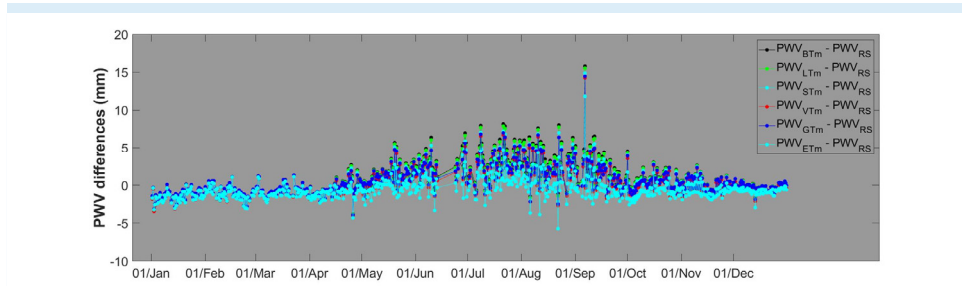
删除的内容: A

删除的内容: is

批注 [jiang27]: GPT2w included

批注 [jiang28]: GPT2w included

Figure 11: RMSEs of PWV_{BTm} , PWV_{STm} , PWV_{VTm} , PWV_{GTm} and PWV_{ETm} compared with PWV_{RS} at 11 IGS stations in 2016. PWV unit is mm.



批注 [jiang29]: GPT2w included

430 Figure 12: PWV differences of PWV_{BTm} , PWV_{LTm} , PWV_{STm} , PWV_{VTm} , PWV_{GTm} and PWV_{ETm} compared with PWV_{RS} at NIRL station in the year 2016. PWV unit is mm.

6. Summary and conclusion

In this study, we estimated T_m using temperature and humidity profile data from IGRA radiosonde data and ERA-Interim reanalysis datasets over a four-years-long period from the year 2009 to 2012. T_s were also extracted from the two data sets.

435 Then we analyzed the relationship between T_s and T_m at each reanalysis grid node and radiosonde station. Analyses indicated that: (1) T_m has a stronger relationship with T_s in mid-high latitudes than in low latitudes; (2) T_s - T_m correlation coefficients are higher over lands than over oceans in low latitudes; (3) the T_s - T_m relationship's variation properties is much more complicated rather than only dependence on point's latitude, and (4) the T_s - T_m relation has strong annual, semiannual, and diurnal variations in many areas.

删除的内容: In low latitudes
删除的内容: .

440 Using global gridded ERA-Interim datasets from 2009 to 2012, we developed static and time-varying global gridded T_s - T_m models. Annual, semiannual, and diurnal variations in T_s - T_m relationship are considered in a time-varying model. Then we evaluated T_m results from different T_s - T_m models and GPT2w model by comparing them with radiosonde data in 2016. Results demonstrate that time-varying global gridded T_s - T_m model has a significant global precision advantage over other global applied models. Average T_m RMSE reduces by about 1 K. The proportion of sites with small biases and RMSEs increases significantly. At over 90% radiosonde sites, time-varying global gridded model has RMSE smaller than 4 K, and the RMSEs

larger than 5 K nearly disappear. On the other hand, there are more than 17% radiosonde sites have RMSEs larger than 5 K in Bevis or latitude-related models. Multiple statistical tests at 5% significance level verify the significant superiority of the new time-varying model at more than 60% of radiosonde sites. Analyses at specific stations also demonstrate that time-varying global model can eliminate large errors in estimated T_m series.

More precise T_s - T_m models also have positive impacts on GPS-PWV retrievals. Regarding the GPS-PWVs using ERA-Interim T_m estimates as references, relative errors of GPS-PWV using time-varying global gridded T_s - T_m models are within 1.0% at more than 74% IGS sites, which is better than other models. The differences between GPS-PWVs and radiosonde PWVs are around 1~5 mm and mainly influenced by comprehensive error sources rather than single T_m . But at some special sites, such differences could decrease by more than 30% in wetter conditions.

According to our experiments, we are confident that the time-varying global gridded T_s - T_m models presented here will help us to retrieve GPS PWV more precisely, and to study precise PWV variations in high temporal resolution as well as T_s observations. Matlab array file consisting of global gridded coefficients in our model, as well as Matlab codes to interpolate coefficients at any given location, are provided as the supplement of this study. It could be useful for researchers and applicants in relevant fields.

Data sets

Radiosonde data: <ftp://ftp.ncdc.noaa.gov/pub/data/igra>

ERA-Interim Project: <https://doi.org/10.5065/D6CR5RD9>

GPS-ZTD Product: <ftp://cddis.gsfc.nasa.gov/pub/gps/products/troposphere/zpd>

Our model Supplement: <https://www.atmos-meas-tech-discuss.net/amt-2018-67/amt-2018-67-supplement.zip>

Acknowledgments

This study is supported by National Natural Science Foundation of China (No. 41604028), the Anhui Provincial Natural Science Foundation (No. 1708085QD83), and the Doctoral Research Start-up Funds Projects of Anhui University (No. J01001966). The authors thank European Centre for Medium-Range Weather Forecasts for providing the ERA-Interim dataset. We also thank the National Centers for Environmental Information for the IGRa datasets and International GNSS Service for the GNSS troposphere products.

Competing interests

The authors declare that they have no conflict of interest.

删除的内容: of

删除的内容: or

删除的内容: to

删除的内容: s

删除的内容: is

删除的内容: convenient to use

References

- Adams, D. K., Barbosa, H. M. J., and De Los Rios, K. P. G.: A Spatiotemporal Water Vapor-Deep Convection Correlation Metric Derived from the Amazon Dense GNSS Meteorological Network, *Monthly Weather Review*, 145, 279-288, 10.1175/mwr-d-16-0140.1, 2017.
- 485 Adler, B., Kalthoff, N., Kohler, M., Handwerker, J., Wieser, A., Corsmeier, U., Kottmeier, C., Lambert, D., and Bock, O.: The variability of water vapour and pre-convective conditions over the mountainous island of Corsica, *Quarterly Journal Of the Royal Meteorological Society*, 142, 335-346, 10.1002/qj.2545, 2016.
- Bevis, M., Businger, S., Herring, T. A., Rocken, C., Anthes, R. A., and Ware, R. H.: GPS meteorology: Remote sensing of atmospheric water vapor using the global positioning system, *Journal of Geophysical Research: Atmospheres*, 97, 15787-15801, 10.1029/92JD01517, 1992.
- Bohm, J., Moller, G., Schindelegger, M., Pain, G., and Weber, R.: Development of an improved empirical model for slant delays in the troposphere (GPT2w), *Gps Solutions*, 19, 433-441, 10.1007/s10291-014-0403-7, 2015.
- Brown, M. B., and Forsythe, A. B.: Robust Tests for the Equality of Variances, *Publications of the American Statistical Association*, 69, 364-367, 1974.
- 495 Byun, S. H., and Bar-Sever, Y. E.: A new type of troposphere zenith path delay product of the international GNSS service, *J. Geodesy*, 83, 367-373, 10.1007/s00190-008-0288-8, 2009.
- Campmany, E., Bech, J., Rodriguez-Marcos, J., Sola, Y., and Lorente, J.: A comparison of total precipitable water measurements from radiosonde and sunphotometers, *Atmospheric Research*, 97, 385-392, 10.1016/j.atmosres.2010.04.016, 2010.
- 500 Chen, P., Yao, W. Q., and Zhu, X. J.: Realization of global empirical model for mapping zenith wet delays onto precipitable water using NCEP re-analysis data, *Geophys. J. Int.*, 198, 1748-1757, 10.1093/gji/ggu223, 2014.
- Ciesielski, P. E., Chang, W. M., Huang, S. C., Johnson, R. H., Jou, B. J. D., Lee, W. C., Lin, P. H., Liu, C. H., and Wang, J. H.: Quality-Controlled Upper-Air Sounding Dataset for TiMREX/SoWMEX: Development and Corrections, *Journal Of Atmospheric And Oceanic Technology*, 27, 1802-1821, 10.1175/2010jtecha1481.1, 2010.
- 505 Haase, J., Ge, M., Vedel, H., and Calais, E.: Accuracy and variability of GPS tropospheric delay measurements of water vapor in the western Mediterranean, *Journal of Applied Meteorology*, 42, 1547-1568, 10.1175/1520-0450(2003)042<1547:AAVOGT>2.0.CO;2, 2003.
- Hogg, R. V., and Ledolter, J.: *Engineering Statistics*, Macmillan, New York, 1987.
- Jade, S., and Vijayan, M. S. M.: GPS-based atmospheric precipitable water vapor estimation using meteorological parameters interpolated from NCEP global reanalysis data, *Journal of Geophysical Research-Atmospheres*, 113, 10.1029/2007jd008758, 2008.
- 510 Jiang, P., Ye, S. R., Chen, D. Z., Liu, Y. Y., and Xia, P. F.: Retrieving Precipitable Water Vapor Data Using GPS Zenith Delays and Global Reanalysis Data in China, *Remote Sensing*, 8, 10.3390/rs8050389, 2016.
- 515 Karabatic, A., Weber, R., and Haiden, T.: Near real-time estimation of tropospheric water vapour content from ground based GNSS data and its potential contribution to weather now-casting in Austria, *Adv. Space Res.*, 47, 1691-1703, 10.1016/j.asr.2010.10.028, 2011.

- Kealy, J., Foster, J., and Businger, S.: GPS meteorology: An investigation of ocean-based precipitable water estimates, *Journal Of Geophysical Research-Atmospheres*, 117, 10.1029/2011jd017422, 2012.
- Lan, Z., Zhang, B., and Geng, Y.: Establishment and analysis of global gridded Tm – Ts relationship model, *Geodesy and Geodynamics*, 7, 101-107, <https://doi.org/10.1016/j.geog.2016.02.001>, 2016.
- 520 Lee, J., Park, J.-U., Cho, J., Baek, J., and Kim, H. W.: A characteristic analysis of fog using GPS-derived integrated water vapour, *Meteorological Applications*, 17, 463-473, 10.1002/met.182, 2010.
- Li, X., Zhang, L., Cao, X. J., Quan, J. N., Wang, T. H., Liang, J. N., and Shi, J. S.: Retrieval of precipitable water vapor using MFRSR and comparison with other multisensors over the semi-arid area of northwest China, *Atmospheric Research*, 172, 83-94, 10.1016/j.atmosres.2015.12.015, 2016.
- 525 Liu, Z. Z., Li, M., Zhong, W. K., and Wong, M. S.: An approach to evaluate the absolute accuracy of WVR water vapor measurements inferred from multiple water vapor techniques, *Journal Of Geodynamics*, 72, 86-94, 10.1016/j.jog.2013.09.002, 2013.
- Lu, C. X., Li, X. X., Nilsson, T., Ning, T., Heinkelmann, R., Ge, M. R., Glaser, S., and Schuh, H.: Real-time retrieval of precipitable water vapor from GPS and BeiDou observations, *J. Geodesy*, 89, 843-856, 10.1007/s00190-015-0818-0, 2015.
- 530 Mahoney, K., Jackson, D. L., Neiman, P., Hughes, M., Darby, L., Wick, G., White, A., Sukovich, E., and Cifelli, R.: Understanding the role of atmospheric rivers in heavy precipitation in the Southeast US, *Monthly Weather Review*, 10.1175/MWR-D-15-0279.1, 2016.
- Means, J. D.: GPS Precipitable Water as a Diagnostic of the North American Monsoon in California and Nevada, *J. Clim.*, 26, 1432-1444, 10.1175/jcli-d-12-00185.1, 2013.
- 535 Ning, T., Wang, J., Elgered, G., Dick, G., Wickert, J., Bradke, M., Sommer, M., Querel, R., and Smale, D.: The uncertainty of the atmospheric integrated water vapour estimated from GNSS observations, *Atmos. Meas. Tech.*, 9, 79-92, 10.5194/amt-9-79-2016, 2016.
- Pacione, R., and Vespe, F.: Comparative studies for the assessment of the quality of near-real-time GPS-derived atmospheric parameters, *Journal of Atmospheric and Oceanic Technology*, 25, 701-714, 10.1175/2007jtecha935.1, 2008.
- 540 Perez-Ramirez, D., Whiteman, D. N., Smirnov, A., Lyamani, H., Holben, B. N., Pinker, R., Andrade, M., and Alados-Arboledas, L.: Evaluation of AERONET precipitable water vapor versus microwave radiometry, GPS, and radiosondes at ARM sites, *Journal Of Geophysical Research-Atmospheres*, 119, 9596-9613, 10.1002/2014jd021730, 2014.
- Raju, C. S., Saha, K., Thampi, B. V., and Parameswaran, K.: Empirical model for mean temperature for Indian zone and estimation of precipitable water vapor from ground based GPS measurements, *Ann. Geophys.*, 25, 1935-1948, 2007.
- 545 Rocken, C., Johnson, J., Van Hove, T., and Iwabuchi, T.: Atmospheric water vapor and geoid measurements in the open ocean with GPS, *Geophysical Research Letters*, 32, 10.1029/2005gl022573, 2005.
- Rohm, W., Yuan, Y. B., Biadegligne, B., Zhang, K. F., and Le Marshall, J.: Ground-based GNSS ZTD/IWV estimation system for numerical weather prediction in challenging weather conditions, *Atmospheric Research*, 138, 414-426, 10.1016/j.atmosres.2013.11.026, 2014.
- 550 Saastamoinen, J.: Atmospheric correction for the troposphere and stratosphere in radio ranging of satellites, *Use of Artificial Satellites for Geodesy*, 15, 274-251, 1972.
- Sheng, P., Mao, J., Li, J., Ge, Z., Zhang, A., Sang, J., Pan, N., and Zhang, H.: *Atmospheric Physics 2ed.*, Peking University Press,

- Beijing, 2013.
- 555 Singh, D., Ghosh, J. K., and Kashyap, D.: Weighted mean temperature model for extra tropical region of India, *Journal of Atmospheric and Solar-Terrestrial Physics*, 107, 48-53, <http://dx.doi.org/10.1016/j.jastp.2013.10.016>, 2014.
- Song, J. J., Wang, Y., and Tang, J. P.: A Hiatus of the Greenhouse Effect, *Sci Rep*, 6, 9, 10.1038/srep33315, 2016.
- Van Baelen, J., and Penide, G.: Study of water vapor vertical variability and possible cloud formation with a small network of GPS stations, *Geophysical Research Letters*, 36, 10.1029/2008gl036148, 2009.
- 560 Wang, J. H., Zhang, L. Y., and Dai, A.: Global estimates of water-vapor-weighted mean temperature of the atmosphere for GPS applications, *Journal of Geophysical Research-Atmospheres*, 110, 10.1029/2005jd006215, 2005.
- Wang, X. M., Zhang, K. F., Wu, S. Q., Fan, S. J., and Cheng, Y. Y.: Water vapor-weighted mean temperature and its impact on the determination of precipitable water vapor and its linear trend, *Journal Of Geophysical Research-Atmospheres*, 121, 833-852, 10.1002/2015jd024181, 2016.
- 565 Wang, X. Y., Song, L. C., and Cao, Y. C.: Analysis of the weighted mean temperature of china based on sounding and ECMWF reanalysis data, *Acta Meteorol. Sin.*, 26, 642-652, 10.1007/s13351-012-0508-2, 2012.
- Yao, Y., Zhang, B., Xu, C., and Yan, F.: Improved one/multi-parameter models that consider seasonal and geographic variations for estimating weighted mean temperature in ground-based GPS meteorology, *J. Geodesy*, 88, 273-282, 10.1007/s00190-013-0684-6, 2014a.
- 570 Yao, Y. B., Zhu, S., and Yue, S. Q.: A globally applicable, season-specific model for estimating the weighted mean temperature of the atmosphere, *J. Geodesy*, 86, 1125-1135, 10.1007/s00190-012-0568-1, 2012.
- Yao, Y. B., Zhang, B., Xu, C. Q., and Chen, J. J.: Analysis of the global T(m)-T(s) correlation and establishment of the latitude-related linear model, *Chinese Science Bulletin*, 59, 2340-2347, 10.1007/s11434-014-0275-9, 2014b.